Engineering 5 (2019) 434–440

Contents lists available at ScienceDirect

Engineering

journal homepage: www.elsevier.com/locate/eng

Research
Deep Matter & Energy—Review

A Breakthrough in Pressure Generation by a Kawai-Type Multi-Anvil Apparatus with Tungsten Carbide Anvils

Takayuki Ishii [a], Zhaodong Liu [a,b], Tomoo Katsura [a,c,*]

[a] Bayerisches Geoinstitut, University of Bayreuth, Bayreuth 95440, Germany
[b] State Key Laboratory of Superhard Materials, Jilin University, Changchun 130012, China
[c] Center for High Pressure Science and Technology Advanced Research, Beijing 100094, China

ARTICLE INFO

Article history:
Received 8 July 2018
Revised 4 January 2019
Accepted 28 January 2019
Available online 26 April 2019

Keywords:
High pressure
Multi-anvil apparatus
Tungsten carbide anvil
Sintered diamond anvil
Lower mantle

ABSTRACT

Expansion of the pressure range of Kawai-type multi-anvil presses (KMAPs) with tungsten carbide (WC) anvils is called for, especially in the field of Earth science. However, no significant progress in pressure generation has been made for 40 years. Our recent studies have expanded the pressure generation of a KMAP with WC anvils to 65 GPa, which is the world record for high-pressure generation in this device and is more than 2.5 times higher than conventional pressure generation. We have also successfully generated pressures of about 50 GPa at high temperatures. This work reviews our recently developed technology for high-pressure generation. High-pressure generation at room temperature and at high temperature was attained by integration of the following techniques: ① a precisely aligned guide-block system, ② a high degree of hardness of the second-stage anvils, ③ tapering of the second-stage anvil faces, ④ a high-pressure cell consisting of materials with a high bulk modulus, and ⑤ high thermal insulation of the furnace. Our high-pressure technology will facilitate investigation of the phase stability and physical properties of materials under the conditions of the upper part of the lower mantle, and will permit the synthesis and characterization of novel materials.

1. Introduction

A multi-anvil press is a static high-pressure apparatus in which a sample is compressed with more than three anvils. The Kawai-type multi-anvil press (KMAP) is one of the most widely used high-pressure apparatuses in the field of geophysics [1]. A main feature of the KMAP is its double-stage compression system, in which pressure is generated by squeezing an octahedral pressure medium by the truncated corners of eight cubic second-stage anvils that are synchronously compressed by six first-stage anvils. The main advantages of the KMAP, in comparison with the other widely used high-pressure apparatus, the diamond anvil cell (DAC), are its much larger sample volumes, more stable temperature over time, and more homogeneous pressure–temperature fields. For example, KMAPs have sample volumes that are three orders of magnitude larger than DACs in the same pressure range, and higher precision by one order of magnitude in pressure and temperature control. These advantages allow the KMAP to yield highly reliable experimental results; therefore, KMAPs have been particularly utilized for the precise determination of the phase relations and high-temperature physical properties of mantle minerals. Recently, KMAPs have also been used in the field of materials science, for the syntheses of novel materials at pressures that cannot be reached by any other large-volume presses [2].

One reason for the wide use of KMAPs in studies of the Earth's interior is that they routinely allow pressures of up to 25 GPa to be generated [3]. Various phase changes in mantle rock-forming minerals occur in this pressure range, which corresponds to depths as low as the uppermost lower mantle in the Earth's interior (~700 km). It was considered for many years that the composition in the deeper parts of the lower mantle is homogeneous, and that no remarkable changes are likely to occur in the phase stabilities and physical properties of the minerals there. Therefore, pressure generation of up to 25 GPa has been sufficient for many researchers.

Recent seismological studies, however, have shown slabs subducting into the lower mantle and settling at a depth of around 1000 km (~40 GPa) [4]. Another study has shown that although mantle plumes from the core-mantle boundary are vertically

* Corresponding author.
E-mail address: tomo.katsura@uni-bayreuth.de (T. Katsura).

https://doi.org/10.1016/j.eng.2019.01.013

straight to a depth of 1000 km, they bend in shallower regions [5]. Thus, it is desirable for KMAPs to be developed such that they can be used to expand the exploration of the chemistry and physics of mantle minerals to pressures greater than 40 GPa.

Improvement of KMAP technology in recent years has enabled pressures of 60 GPa to be reached by utilizing sintered diamond (SD) second-stage anvils [6,7]. The latest technology of SD anvils makes it possible to generate pressures over 100 GPa [8,9]. However, the cost of SD anvils is much higher than that of tungsten carbide (WC) anvils. Special techniques for manufacturing anvils and high-pressure cell parts in combination with a precisely aligned guide-block system are also necessary for successful high-pressure and high-temperature generation. Moreover, the edge lengths of SD anvil cubes are 10–14 mm—less than half that of WC anvils (26–32 mm). Therefore, research groups that can practically conduct experiments using SD anvils are limited. In contrast, WC second-stage anvils have been widely utilized in KMAPs because they are less expensive and more tractable than SD anvils. For these reasons, we have made improvements in a KMAP with WC anvils to allow it to generate pressures greater than 40 GPa [10,11]. Other researchers have recently developed KMAP technology with WC anvils that can achieve pressures of up to 50 GPa at room temperature [12]; however, our particular focus is on high-pressure generation under high temperatures.

This paper reviews our recently developed methods for pressure generation up to 65 GPa, which greatly exceeds the conventional limitation of pressure generation in KMAPs with WC anvils. In this paper, we refer to pressures greater than 40 GPa as "ultrahigh pressures."

2. Methods

2.1. Guide-block system

The first- and second-stage anvils compress cubic and octahedral spaces, respectively. High pressures are sealed by gaskets made of pyrophyllite. Ideally, the thicknesses of the gaskets must be identical for ultrahigh-pressure generation, because any difference in the thickness weakens the high-pressure sealing by the gaskets. For this purpose, the cubic and octahedral compression spaces must be highly symmetrical.

Conventional KMAPs employ first-stage anvils and a guide-block system, in which a second-stage anvil assembly is vertically oriented in the [111] direction [13–15] by placing two sets of three first-stage anvils on the upper and lower sides. Although six first-stage anvils are simply placed in a guide cylinder in the Walker module, two sets of three first-stage anvils are fixed in the upper and lower guide blocks in other types of KMAP. These two sets of first-stage anvils are driven by a uniaxial press. Applied press loads in these configurations, however, tend to distort the cubic compression space rhombohedrally and cause blow-out when attempting to generate ultrahigh pressures.

In order to prevent rhombohedral distortion, we have employed the Osugi-type guide-block system [16], which is also known as the DIA-type system[†] in the high-pressure science community (Fig. 1). The Osugi-type system consists of upper and lower guide blocks with four 45° slopes, on which four sliding wedges are located. Each of the guide blocks and sliding wedges is equipped with a first-stage anvil. The uniaxial force causes the four wedges to advance, so the cubic space is synchronously compressed by the six first-stage anvils in the [100] directions. This configuration causes no rhombohedral distortion.

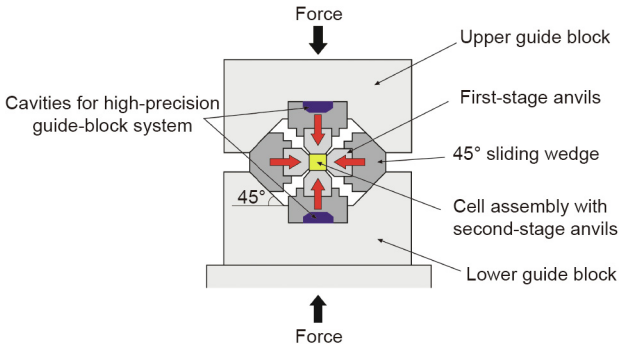

Fig. 1. Schematic drawings of the Osugi (DIA)-type compression system. A uniaxial press compresses guide blocks and finally creates a cubic compression space surrounded by six first-stage anvils, each of which compresses the cubic space in the [100] directions. Cavities are made in a KMAP with the high-precision guide-block system.

The principal issue with the Osugi-type system is that the cubic compression space is tetragonally distorted by the application of press loads, due to the difference in supporting strength for the first-stage anvils between the guide blocks and the sliding wedges. The distortion of the cubic space varies vertically and horizontally as the press load increases. This causes a difference in the vertical and horizontal gasket thickness between the anvil gaps, and increases the frequency of blow-out. To solve this issue, the supporting strengths for the upper and lower first-stage anvils were adjusted by manufacturing cavities in the guide blocks (Fig. 1). As a result, the dimension of the compression space in the horizontal and vertical directions remains essentially identical under any press load. We hereafter refer to the Osugi-type guide-block system with this improvement as the "high-precision guide-block system."

To date, three KMAPs with the high-precision guide-block system have been built in the world: The first is SPEED-Mk.II in the BL04B1 beamline at the synchrotron radiation facility of SPring-8, Japan [17]; the second is MADONNA-1500 at the Geodynamic Research Center at Ehime University, Japan [18]; and the third is IRIS-15 at the Bayerisches Geoinstitut University of Bayreuth, Germany [10]. Other KMAPs have also been constructed with the Osugi-type guide-block system, but the anvil-supporting strengths of these systems have not been adjusted. One example of the latter is SPEED-1500, which is also in the BL04B1 beamline at the SPring-8 synchrotron radiation facility. The horizontal dimensions of the cubic compression space in SPEED-1500 increase relative to the vertical dimensions against a press load (+13 $\mu m \cdot MN^{-1}$ [17]). In contrast, this rate was suppressed to +4, +1.6, and –0.07 $\mu m \cdot MN^{-1}$ in the cases of SPEED-Mk.II, MADONNA-1500, and IRIS-15, respectively. Note that the guide blocks of SPEED-Mk.II were replaced by those of MADONNA-1500, and SPEED-Mk.II is now called SPEED-Mk.II-D. The highest pressure generated by SPEED-1500 using SD anvils is 44 GPa [19], whereas a pressure of 120 GPa has been generated by SPEED-Mk.II-D [8,9], clearly demonstrating the usefulness of the high-precision guide-block system for ultrahigh-pressure generation.

2.2. The first-stage anvils

The first-stage anvils are made of hardened steel in order to compress a KMAP assembly in combination with the second-stage WC anvils. As reported in Refs. [10,11], the pressure increases

[†] This guide-block system was developed by Jiro Osugi's laboratory at the Department of Chemistry, Kyoto University, in order to generate pressures up to 10 GPa in 1000 mm^3 by means of a uniaxial press. Before the efforts of these researchers, multi-anvil presses had the same number of rams as those of anvils, along with a huge chassis. The apparatus by Osugi et al. is the origin of current uniaxial multi-anvil presses.

rapidly under press loads of up to 4 MN, and then gradually under higher press loads at least up to 15 MN. Therefore, it is useful for a hydraulic system and press chassis to allow the application of press loads up to 15 MN. The second-stage anvils are frequently broken during ultrahigh-pressure generation, which limits their practical use in high-pressure research. Hence, the size of second-stage anvils should be minimized. Assuming that the compressional strength of hardened steel for second-stage anvils is 2 GPa, the truncated edge length (TEL) of first-stage anvils should be 50 mm. Thus, first-stage anvils usually have this TEL. In order to fit the TEL of first-stage anvils, second-stage anvils are usually around 26 mm in edge length.

2.3. The second-stage anvils

Needless to say, a harder anvil material allows higher pressure generation. Therefore, high-pressure generation in a KMAP significantly depends on the mechanical properties of the WC adopted for the second-stage anvils. Table 1 [20,21] lists the mechanical properties of various grades of WC. Conventional WC anvils have a Vickers hardness (HV) of less than HV = 2000, which can only generate pressures up to 25 GPa [3]. In this work, we used WC with a high hardness of HV > 2000. Although these WC anvils can easily be broken by blow-out during decompression, their use is essential for generating ultrahigh pressures above 30 GPa. The TEL of the second-stage anvils is another important parameter in generating ultrahigh pressure, because the efficiency of pressure generation increases with decreasing TEL size. We empirically decided to use a TEL size of 1.5 mm. Higher pressures could be generated if smaller truncations were adopted.

Pressure generation using any anvil material is limited by the anvil yielding, particularly around a truncation. If the compression space formed by second-stage anvils is not decreased due to yielding of the truncated corners of the anvils, the sample pressure does not increase despite the addition of a press load. We introduced tapering to the anvils in order to reduce this yielding. Three anvil faces around a truncation of second-stage anvils were tapered by 1°, which was determined empirically (Fig. 2(a)). This is essentially the same technology as bevel processing in DACs, by which pressures greater than 200 GPa were first achieved in a DAC [22]. Fig. 2(b) and Fig. 2(c), respectively, show schematic cross-sections of anvil tops for flat and tapered anvils under pressure. The anvil-tapering technique was pioneered in a KMAP about 40 years ago [23]. However, the pressure generation of that system was limited to about 30 GPa due to anvil hardness limitation at that time. Using IRIS-15, we conducted pressure generation tests at room temperature for flat and 1° tapered anvils with a truncation of 1.5 mm (Grade TF05) (Fig. 3). The pressures against the press load were determined based on changes in electric resistance corresponding to the following phase transitions: zinc sulfide (ZnS) semiconductor–metal (15.6 GPa [1,24]), gallium phosphide (GaP) semiconductor–metal (23 GPa [1,24]), zirconium (Zr) α–ω (8 GPa [25,26]), and Zr ω–β (34 GPa [25,26]). The press load for the ω–β transitions of Zr was reduced by 30% (from 10.8 to 7.5 MN) by the adoption of anvil tapering; higher efficiency in pressure generation is achieved by anvil tapering at relatively high press loads.

2.4. Cell assembly

Cell assembly setup is another important factor in the generation of ultrahigh pressures. Fig. 4 shows cross-sections of the cell assemblies used for high-pressure generation tests at room temperature and high temperature. An octahedron with edge lengths of 5.7 mm made of magnesium oxide (MgO) doped with 5 wt% of chromium(III) oxide (Cr_2O_3) was adopted for a pressure medium. A sample was placed at the center of the pressure medium. High pressures are generated by the volume decrease of a sample chamber. Therefore, if the materials in a high-pressure cell have high compressibility, the pressure increase is limited. For this reason, the sample was sandwiched with aluminum oxide (Al_2O_3) rods, because Al_2O_3 has a higher bulk modulus (~240 GPa [27]) than MgO (~160 GPa [27]).

Table 1
Mechanical properties of WCs.

Company	Grade	Vickers hardness, HV	Rockwell hardness, HRA	Compressive strength (GPa)
Tungaloy	F	1950[a]	93.4[a]	7.0[a]
Hawedia	HA-7% Co	1770[a]	93.0[a]	6.8[a]
Fujiloy	TF05	2400 [20]	95.1 [21]	> 8.0 [21]
	TJS01	2700 [20]	97.8 [21]	> 8.0 [21]

[a] These are in the catalogues of the producing companies.

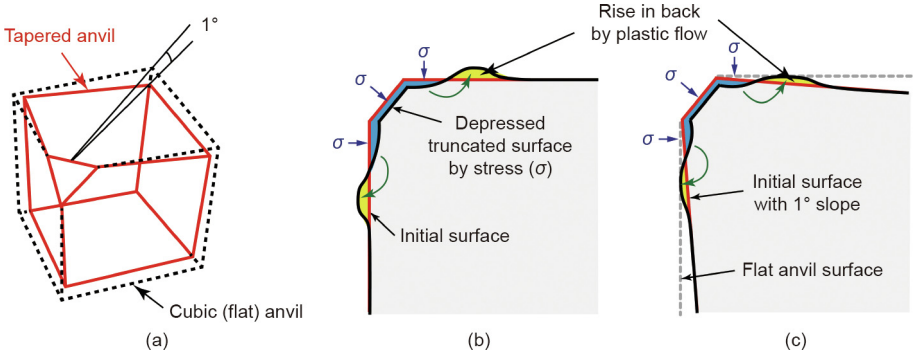

Fig. 2. Schematic illustrations of a second-stage anvil. (a) Geometry of cubic (flat) and tapered anvils. The dashed box indicates the shape of a flat anvil, while the solid box represents a 1° tapered anvil. (b, c) Anvil deformation under high pressure for (b) a flat anvil and (c) a tapered anvil. In (c), dashed lines represent the surfaces of the flat anvil. σ represents simplified stress from the confining pressure (small blue arrow).

For cell assembly for high-temperature experiments (Fig. 4(b)), a cylindrical rhenium (Re) or molybdenum (Mo) foil was adopted as a heater that could directly accommodate the sample material in the form of a sample capsule. The lighter element, Mo, was used as a heater for *in situ* X-ray diffraction experiments due to its higher X-ray transparency (Fig. 4(c)). Mo electrodes were used to electrically connect the heater and the second-stage anvils. At high temperatures, softening of the gaskets and pressure media causes pressure drops, because it prompts material flows through anvil gaps, and decreases the amount of materials confined in the compression spaces. We suppressed this softening by replacing significant parts of the Cr_2O_3-doped MgO pressure medium outside of the furnace with a $LaCrO_3$ thermal insulator. Temperatures were measured at the surface of the heater with a W97%Re3%–W75%Re25% thermocouple that was electrically insulated from the $LaCrO_3$ by Al_2O_3 tubes. For *in situ* X-ray diffraction experiments, Al_2O_3 X-ray windows with a diameter of 0.5 mm were set along the X-ray path outside of the furnace to suppress X-ray absorption by the pressure medium of Cr_2O_3-doped MgO and the thermal insulator of $LaCrO_3$ (Fig. 4(c)). As shown later, however, these X-ray windows greatly decrease the sample pressure.

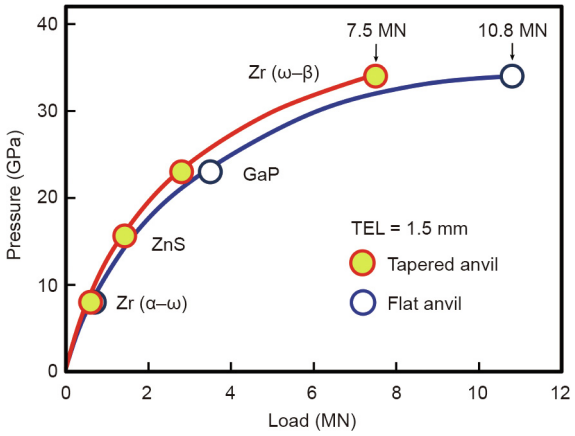

Fig. 3. Pressures generated with tapered (yellow-filled red circles) and flat (open blue circles) anvils at room temperature. ZnS, GaP, and Zr were the pressure calibrants.

2.5. Pressure determination for in-house and in situ experiments and sample preparation

In conventional in-house experiments, generated pressures are estimated based on pressure calibration against the press load through the detection of phase transitions. However, one of the problems affecting KMAPs for pressures above 30 GPa is the irreproducibility of generated pressures against the press load, especially at high temperatures. For this reason, the pressures must be evaluated during each run. Since the Al_2O_3 content in bridgmanite (Brg, $MgSiO_3$) coexisting with corundum (Cor, Al_2O_3) increases with pressure [28], generated pressures were estimated by measuring the composition of aluminous Brg in a run product after recovery using an electron microprobe analyzer.

A sample with the composition $Mg_3Al_2Si_3O_{12}$, which is known as pyrope (Py), was used as the pressure calibrant. Py is phase stable at pressures above 2 GPa. At pressures higher than 26 GPa and at high temperatures, Py transforms to Brg (+ Cor), which results in a volume change greater than 10% [29] and causes a pressure drop. To suppress this pressure drop, we loaded sintered akimotoite with a Py composition (Py–Ak), which is one of the low-pressure phases of Brg and has a volume that is 8% smaller than that of Py. The synthesis of the Py–Ak was performed with an $Mg_3Al_2Si_3O_{12}$-compositional glass at 26 GPa and 1170 K [30]. In order to make the glass, an oxide mixture with the composition $Mg_3Al_2Si_3O_{12}$—prepared using MgO, Al_2O_3, and SiO_2 oxides—was melted at 1950 K for 1 h, and then rapidly cooled in water. The synthesis of Py–Ak can be only conducted at relatively low temperatures up to 1170 K; this kind of phase has a high reactivity at

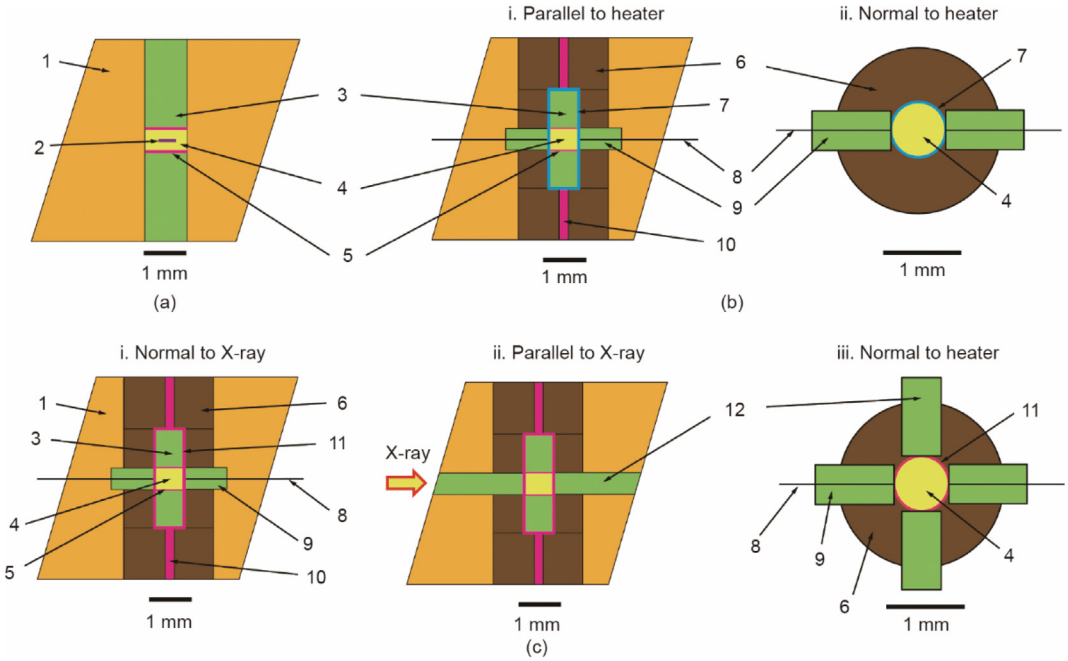

Fig. 4. Cross-sections of cell assemblies in combination with 1° tapered anvils with a TEL of 1.5 mm for room temperature and high temperatures. (a) Room temperature cell for *in situ* X-ray diffraction experiment; (b) high temperature cell for in-house experiment; (c) high temperature cell for *in situ* X-ray diffraction experiment. 1: 5 wt% Cr_2O_3-doped MgO pressure medium with 5.7 mm edge length; 2: gold (Au) foil; 3: dense alumina; 4: sample; 5: Mo disc; 6: $LaCrO_3$ thermal insulator; 7: Re heater; 8: W97%Re3%–W75%Re25% thermocouple; 9: dense alumina tube; 10: Mo electrode; 11: Mo heater; 12: dense alumina X-ray window.

higher pressures and temperatures. This pre-synthesis technique should be conducted for any samples in order to make a dense starting sample, which is synthesized at a lower temperature than the target temperature for an objective phase. In addition, the calibrant should be practically put together with a sample at a position where a thermocouple measures temperature.

A pressure calibrant for an *in situ* X-ray diffraction experiment was prepared by mixing sintered MgO with 5 wt% gold (Au) at 2 GPa and 1300 K for 1 h. Although these materials do not occur during any phase transition in our investigated pressure–temperature range, sintering is useful to suppress deformation of the sample part during compression and to efficiently generate high pressure due to low porosity.

3. Pressure generation at room temperature

Fig. 5 [10,31] shows the results of pressure generation at ambient temperature by the technology described above using grade TF05 and TJS01 anvils. Generated pressures were determined by means of *in situ* X-ray diffraction with a pressure calibrant of Au, based on equations of state from Ref. [32]. Using TF05 anvils, we reached a pressure of 43 GPa at 15 MN, which was the maximal press load applicable. This pressure is much higher than that generated by conventional KMAP technology (~25 GPa). Using TJS01 anvils, which are much harder than TF05 anvils, an even higher pressure of 64 GPa was achieved. This pressure is 2.5 times higher than that achieved using the conventional technique. If anvil tapering is not adopted, the pressure-increase rates will be close to zero under relatively high press loads (e.g., 0.2 GPa·MN^{-1} above 9 MN) because of anvil deformation [11,12]. However, the increase rate in our experiments remained at 1.5 GPa·MN^{-1} above 9 MN, thanks to the anvil tapering.

4. High-pressure generation at high temperature

High-pressure generation using TF05 anvils at 2000 K was examined based on the Al_2O_3 content in Brg (Fig. 6). At 6 MN, the aluminum (Al) number in Brg was 1.59(2) on the 12-oxygen basis, which suggests a generated pressure of 36 GPa. Furthermore, we

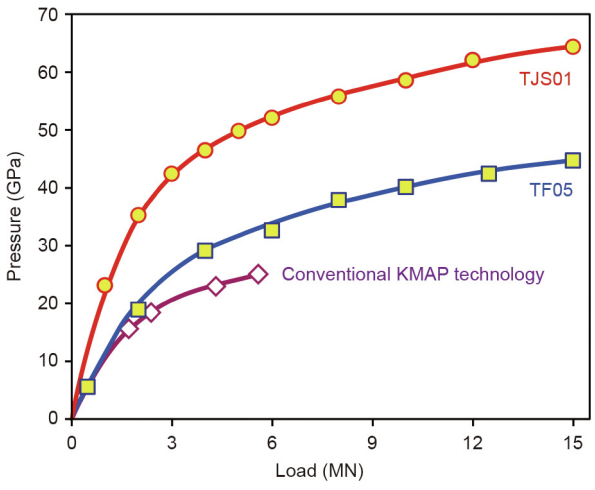

Fig. 5. Pressure generations at room temperature using 1.5 mm TEL hard WC anvils (TF05 and TJS01 grades), compared with pressure generation by conventional KMAP technology using 1.5 mm TEL conventional WC anvils (Tungaloy F grade) [31]. Pressure generation using TJS01 anvils was examined with the cell assembly shown in Fig. 4(a). A cell assembly without an Al_2O_3 X-ray window and with $LaCrO_3$ replaced with Al_2O_3 in Fig. 4(c) was used for the pressure generation tests using TF05 anvils (see Ref. [10] for details).

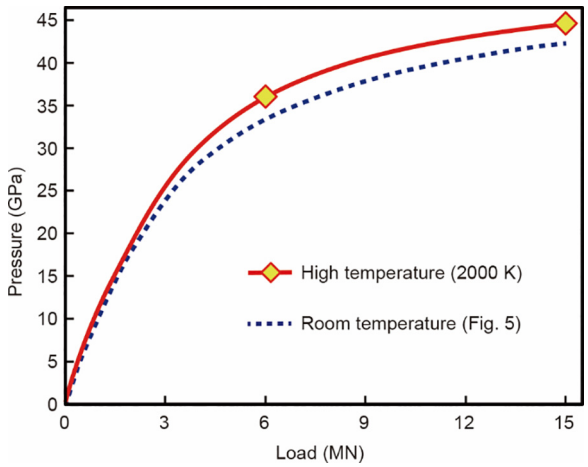

Fig. 6. Pressure generation using 1.5 mm TEL anvils with 1° tapering (TF05 grade) at room temperature (dashed blue curve) and at a high temperature of 2000 K (solid red curve). The cell assembly shown in Fig. 4(b) was used for the high-temperature pressure generation test.

synthesized a $LiNbO_3$ (LN)-type phase with the Py composition [Al = 1.99(2)] [29] at 15 MN, which indicates a generated pressure of 45 GPa. Compared with pressure generation at ambient temperature, pressure generation at high temperature is more effective. We examined the effects of thermal insulation on pressure generation by *in situ* X-ray diffraction. When we used a cell assembly without a thermal insulator, a generated pressure of 43 GPa at ambient temperature dramatically decreased to 36 GPa at 1100 K; the experiment then failed by blow-out. This result is likely due to the softening of cell materials (e.g., the gasket and pressure medium), as mentioned in Section 2.3. Thus, efficient pressure generation at high temperature requires thermal insulation in order to maximize the heating efficiency and achieve a successful result.

We also examined pressure variation with tapered TJS01 anvils while the temperature was increased. For this experiment, we adopted *in situ* X-ray diffraction because the Al content in Brg has been calibrated only up to 45 GPa; thus, no appropriate pressure calibrant is available above 50 GPa for in-house experiments. After reaching 15 MN at room temperature, we conducted stepwise heating and pressure measurements at temperatures up to 2000 K. Fig. 7 [33,34] shows the change in pressure upon heating. The sample pressures drastically decreased with increasing temperature. However, pressures were maintained over 50 GPa up to 1600 K, and a pressure of 48 GPa was still achieved at 2000 K. The reason for the drastic pressure drop is likely the high heat flow from the heater through the Al_2O_3 X-ray window (Fig. 4(c)), which has a thermal conductivity (~7 W·(m·K)$^{-1}$ at 1100 K and 1 atm (1 atm = 101 325 Pa)) much higher than that of $LaCrO_3$ (~2 W·(m·K)$^{-1}$ at 1100 K and 1 atm) [33]. Improvements in the high-temperature generation technique are therefore necessary in order to suppress pressure drops.

It is notable that in most previous experiments, ultrahigh-pressure generation by KMAP was conducted at relatively low temperatures of 300–1500 K [7,8,12]. In contrast, our pressure generation of 48 GPa was achieved at a temperature of 2000 K, which is within the range of expected mantle temperatures (1900–2100 K) [34,35]. Therefore, the simultaneous generation of mid-mantle pressure and temperature in the current work is valuable for practical investigations of the structure, dynamics, and evolution of the mid-mantle. Furthermore, we emphasize that the maximum pressure generated with the TF05 anvils was increased by heating using the assembly without an X-ray window, due to the effect of thermal pressure by high thermal insulation.

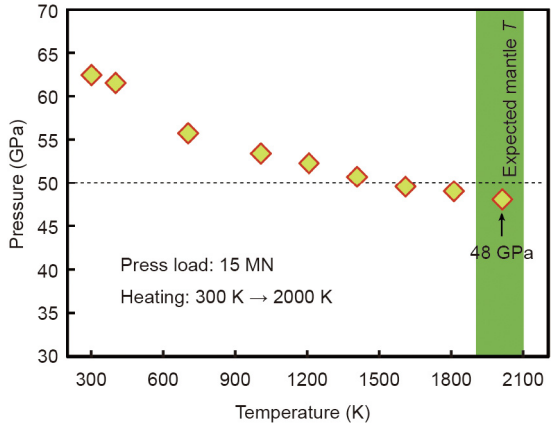

Fig. 7. Pressure variation with increasing temperature to 2000 K using 1.5 mm TEL TJS01 tapered anvils. The cell assembly shown in Fig. 4(c) was used in this test. The band at 1900–2100 K indicates the expected temperatures (T) in the upper part of the lower mantle [33,34].

Therefore, it is expected that TJS01 anvils would allow the generation of much higher pressures than 48 GPa at high temperatures around 2000 K if a cell assembly without X-ray windows was used.

5. Applications

We applied the ultrahigh-pressure technology described in this work to the mineral chemistry of lower-mantle minerals [29,36]. As mentioned above, we successfully synthesized an extremely pure LN-type $Mg_3Al_2Si_3O_{12}$ aggregate with a length of 0.5 mm and diameter of 0.5 mm at 45 GPa and 2000 K in order to refine the structure of this compound by Rietveld analysis using synchrotron powder X-ray diffraction [29]. This work clarified the transformation mechanism of the LN phase from the perovskite structure and suggested application as a possible indicator of shock conditions of meteorites around 45 GPa and 2000 K.

We measured the solubility of the $MgAlO_{2.5}$ component in Brg, which produces oxygen vacancy in the perovskite structure and may accommodate water and noble gases such as argon, at pressures up to 40 GPa and a temperature of 2000 K [36]. We showed that this component rapidly decreases with pressure and becomes virtually absent at pressures above 40 GPa (Fig. 8). These results

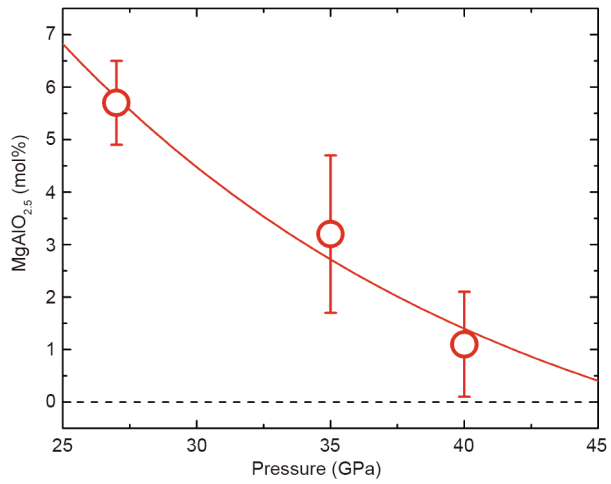

Fig. 8. The $MgAlO_{2.5}$ component in $MgSiO_3$ bridgmanite as a function of pressure at a temperature of 2000 K. The $MgAlO_{2.5}$ component rapidly decreases with pressure and becomes virtually zero at pressures above 40 GPa.

suggest a dry lower mantle at depths greater than 1000 km, at least, because the decrease of this component in Brg, which is a dominant mineral in the lower mantle, will reduce water solubility as an $MgHAlO_3$ component. In addition, this characteristic of Brg suggests a highly viscous lower mantle at depths greater than 1000 km, in comparison with the shallower part of the lower mantle. Because diffusion creep—which is controlled by diffusion coefficient and grain size—would be an essential creep mechanism in Brg under lower mantle conditions due to a seismically isotropic lower mantle [37], a decrease of the point defect concentration in Brg as an $MgAlO_{2.5}$ component with pressure can lead to an increase of the viscosity of Brg with pressure. This expected high viscosity may explain slab stagnation around a depth of 1000 km [4]. Thus, the technique presented here was used to produce important conclusions for the physics, chemistry, and dynamics of the lower mantle. Our technology will allow measurements of the elasticity and elemental diffusivity of lower-mantle minerals, which will contribute to a better understanding of the physics and chemistry of the lower mantle.

6. Conclusion

In this work, we demonstrated pressure generation of up to 65 GPa in a KMAP with WC anvils, by integrating the high-pressure technology developed to date. The adoption of special second-stage WC anvils with high hardness and tapered processing, a material with high incompressibility for pressure transmission, and appropriate thermal insulation effectively enhanced the pressure generation. Maximal sample pressures of 64 and 48 GPa were achieved at ambient temperature and at a high temperature of 2000 K, respectively. Thus, our advanced technology opens a window to investigate the phase stability and physical properties of materials under the conditions of the upper part of the lower mantle, and to explore and characterize novel materials.

Acknowledgements

This work has been supported by an Alexander von Humboldt Postdoctoral Fellowship to T. Ishii. We appreciate M. Akaogi for providing data on pressure generation with Tungaloy F grade anvils. The project leading to this application has received funding from the European Research Council (ERC) under the European Union's Horizon 2020 research and innovation program (787527).

Compliance with ethics guidelines

Takayuki Ishii, Zhaodong Liu, and Tomoo Katsura declare that they have no conflict of interest or financial conflicts to disclose.

References

[1] Ito E. Theory and practice—multianvil cells and high-pressure experimental methods. In: Schubert G, Romanowicz B, Dziewonski A, editors. Treatise on geophysics 2. San Diego: Elsevier; 2007. p. 197–230.
[2] Ovsyannikov SV, Bykov M, Bykova E, Kozlenko DP, Tsirlin AA, Karkin AE, et al. Charge-ordering transition in iron oxide Fe_4O_5 involving competing dimer and trimer formation. Nat Chem 2016;8(5):501–8.
[3] Keppler H, Frost D. Introduction to minerals under extreme conditions. In: Miletich R, editor. Mineral behavior at extreme conditions. Budapest: Eötvös University Press; 2005. p. 1–30.
[4] Fukao Y, Obayashi M. Subducted slabs stagnant above, penetrating through, and trapped below the 660 km discontinuity. J Geophys Res 2013;118(11):5920–38.
[5] French SW, Romanowicz B. Broad plumes rooted at the base of the Earth's mantle beneath major hotspots. Nature 2015;525(7567):95–9.
[6] Wang F, Tange Y, Irifune T, Funakoshi K. P–V–T equation of state of stishovite up to mid-lower mantle conditions. J Geophys Res 2012;117:B06209.
[7] Tange Y, Irifune T, Funakoshi K. Pressure generation to 80 GPa using multianvil apparatus with sintered diamond anvils. High Press Res 2008;28:245–54.

[8] Yamazaki D, Ito E, Yoshino T, Tsujino N, Yoneda A, Guo X, et al. Mbar generation in the Kawai-type multianvil apparatus and its application to compression of $(Mg_{0.92}Fe_{0.08})SiO_3$ perovskite and stishovite. Phys Earth Planet Inter 2014;228:262–7.
[9] Yamazaki D, Ito E, Yoshino T, Tsujino N, Yoneda A, Gomi H, et al. High-pressure generation in the Kawai-type multianvil apparatus equipped with tungsten-carbide anvils and sintered-diamond anvils, and X-ray observation on $CaSnO_3$ and $(Mg,Fe)SiO_3$. Comp Rend Geosci. In press.
[10] Ishii T, Shi L, Huang R, Tsujino N, Druzhbin D, Myhill R, et al. Generation of pressures over 40 GPa using Kawai-type multi-anvil press with tungsten carbide anvils. Rev Sci Instrum 2016;87:024501.
[11] Ishii T, Yamazaki D, Tsujino N, Xu F, Liu Z, Kawazoe T, et al. Pressure generation to 65 GPa in a Kawai-type multi-anvil apparatus with tungsten carbide anvils. High Press Res 2017;37(4):507–15.
[12] Kunimoto T, Irifune T, Tange Y, Wada K. Pressure generation to 50 GPa in Kawai-type multianvil apparatus using newly developed tungsten carbide anvils. High Press Res 2016;36:1–8.
[13] Kawai N, Togaya M, Onodera A. A new device for pressure vessels. Proc Jpn Acad 1973;49(8):623–6.
[14] Ohtani E, Irifune T, Hibberson WO, Ringwood AE. Modified split-sphere guide block for practical operation of a multiple-anvil apparatus. High Temp High Press 1987;19(5):523–9.
[15] Walker D, Carpenter MA, Hitch CM. Some simplifications to multianvil devices for high pressure experiments. Am Miner 1990;75(9–10):1020–8.
[16] Osugi J, Shimizu K, Inoue K, Yasunami K. A compact cubic anvil high pressure apparatus. Rev Phys Chem Jpn 1964;34(1):1–6.
[17] Katsura T, Funakoshi K, Kubo A, Nishiyama N, Tange Y, Sueda Y, et al. A large-volume high-pressure and high-temperature apparatus for *in situ* X-ray observation, "SPEED-Mk.II". Phys Earth Planet Inter 2004;143–144:497–506.
[18] Irifune T. Frontiers in deep earth mineralogy using new large-volume D-DIA and KMA apparatus. Rev High Press Sci Tech 2010;20(2):158–65.
[19] Kubo A, Ito E, Katsura T, Shinmei T, Yamada H, Nishikawa O, et al. *In situ* X-ray observation of iron using Kawai-type apparatus equipped with sintered diamond: absence of β phase up to 44 GPa and 2100 K. Geophys Res Lett 2003;30(3):1126.
[20] Irifune T, Adachi Y, Fujino K, Ohtani E, Yoneda A, Sawamoto H. A performance test for WC anvils for multianvil apparatus and phase transformations in some aluminous minerals up to 28 GPa. In: Syono Y, Manghnani MH, editors. High-pressure research: application to earth and planetary sciences. Washington, DC: American Geophysical Union; 1992. p. 43–50.
[21] Wada K. Tungsten carbide based hardmetals used for high pressure experiment. Rev High Press Sci Tech 2018;28(1):9–16.
[22] Mao HK, Bell PM. Generation of static pressures to 1.5 Mbar. Carnegie Inst Washington 1977;76:644–6.
[23] Ito E. The absence of oxide mixture in high-pressure phases of Mg-silicates. Geophys Res Lett 1977;4(2):72–4.
[24] Dunn KJ, Bundy FP. Materials and techniques for pressure calibration by resistance-jump transitions up to 500 kilobars. Rev Sci Instrum 1978;49(3):365–70.
[25] Tange Y, Takahashi E, Funakoshi KI. *In situ* observation of pressure-induced electrical resistance changes in zirconium: pressure calibration points for the large volume press at 8 and 35 GPa. High Press Res 2011;31(3):413–8.
[26] Ono S, Kikegawa T. Determination of the phase boundary of the omega to beta transition in Zr using *in situ* high-pressure and high-temperature X-ray diffraction. J Solid State Chem 2015;225:110–3.
[27] Soga N, Anderson OL. High-temperature elastic properties of polycrystalline MgO and Al_2O_3. J Am Ceram Soc 1966;49:355–9.
[28] Liu Z, Nishi M, Ishii T, Fei H, Miyajima N, Ballaran TB, et al. Phase relations in the system $MgSiO_3$–Al_2O_3 up to 2300 K at lower mantle pressures. J Geophys Res 2017;122(10):7775–88.
[29] Ishii T, Sinmyo R, Komabayashi T, Ballaran TB, Kawazoe T, Miyajima N, et al. Synthesis and crystal structure of $LiNbO_3$-type $Mg_3Al_2Si_3O_{12}$: a possible indicator of shock conditions of meteorites. Am Miner 2017;102(9):1947–52.
[30] Kubo A, Akaogi M. Post-garnet transitions in the system $Mg_4Si_4O_{12}$–$Mg_3Al_2Si_3O_{12}$ up to 28 GPa: phase relations of garnet, ilmenite and perovskite. Phys Earth Planet Inter 2000;121(1–2):85–102.
[31] Kubo A. High-pressure experimental study on garnet-perovskite transition in the system $MgSiO_3$–Al_2O_3 [dissertation]. Tokyo: Gakushuin University; 1999.
[32] Tsuchiya T. First-principles prediction of the *P*–*V*–*T* equation of state of gold and the 660-km discontinuity in Earth's mantle. J Geophys Res 2003;108:2462.
[33] Kingery WD, Francl J, Coble RL, Vasilos T. Thermal conductivity: X, data for several pure oxide materials corrected to zero porosity. J Am Ceram Soc 1954;37:107–10.
[34] Akaogi M, Ito E, Navrotsky A. Olivine-modified spinel-spinel transitions in the system Mg_2SiO_4–Fe_2SiO_4: calorimetric measurements, thermochemical calculation, and geophysical application. J Geophys Res 1989;94:15671–85.
[35] Katsura T, Yoneda A, Yamazaki D, Yoshino T, Ito E. Adiabatic temperature profile in the mantle. Phys Earth Planet Inter 2010;183:212–8.
[36] Liu Z, Ishii T, Katsura T. Rapid decrease of $MgAlO_{2.5}$ component in bridgmanite with pressure. Geochem Perspect Lett 2018;5:12–8.
[37] Wookey J, Kendall JM, Barruol G. Mid-mantle deformation inferred from seismic anisotropy. Nature 2002;415(6873):777–80.